Using Computational Fluid Dynamics Analysis to Characterize Local Hemodynamic Features of Middle Cerebral Artery Aneurysm Rupture Points

Q3 *Keiji Fukazawa[1], Fujimaro Ishida[1], Yasuyuki Umeda[2], Yoichi Miura[2], Shinichi Shimosaka[1], Satoshi Matsushima[2], Waro Taki[2], Hidenori Suzuki[2]*

Key words
- Computational fluid dynamics
- Local hemodynamics
- Rupture point
- Ruptured cerebral aneurysm
- Wall shear stress

Abbreviations and Acronyms
3D-CTA: Three-dimensional computed tomographic angiography
CFD: Computational fluid dynamics
CT: Computed tomography
MCA: Middle cerebral artery
NWSS: Normalized wall shear stress
WSS: Wall shear stress

From the [1]Department of Neurosurgery, NHO Mie Chuo Medical Center, Mie; and [2]Department of Neurosurgery, Mie University Graduate School of Medicine, Tsu, Mie, Japan

To whom correspondence should be addressed: Keiji Fukazawa, M.D. [E-mail: fukaz1977@yahoo.co.jp]

Citation: World Neurosurg. (2013). http://dx.doi.org/10.1016/j.wneu.2013.02.012

Journal homepage: www.WORLDNEUROSURGERY.org

Available online: www.sciencedirect.com

■ OBJECTIVE: **Although rupture of cerebral aneurysms typically occurs at the fragile wall at the apex or pole, some aneurysms rupture through the body or the neck. The purpose of this study was to clarify the association between aneurysm rupture points and hemodynamic features through the use of computational fluid dynamics (CFD) analysis.**

■ METHODS: **Twelve ruptured middle cerebral artery bifurcation aneurysms were analyzed by 3-dimensional computed tomographic angiography and CFD. Rupture points were evaluated on intraoperative videos by 3 independent neurosurgeons. Wall shear stress (WSS) was calculated at the rupture point, aneurysm dome, and parent artery. Intra-aneurysmal flow patterns were evaluated with cross-sectional velocity vector planes that included the rupture points.**

■ RESULTS: **The mean WSS at the rupture point (0.29 Pa) was significantly lower than that at the dome (2.27 Pa) and the parent artery (8.19 Pa) ($P < .01$). All rupture points were located within the area of WSS ≤ 11.2% of the WSS at the parent artery. WSS at the rupture point was correlated with the minimum WSS at the dome ($r = 0.64$, $P < .05$), but not with aneurysm size ($r = 0.26$) or the aspect ratio ($r = 0.16$). Flow patterns revealed that all rupture points were located in lower-velocity area, which was associated with complex flow patterns and/or deviating necks.**

Q1

■ CONCLUSIONS: **This study highlights the relationship between the local hemodynamic features and the rupture points observed during the microsurgical clipping. CFD may determine a rupture point of aneurysms using the feature of markedly low WSS.**

INTRODUCTION

Noninvasive cerebrovascular imaging techniques, such as magnetic resonance angiography and 3-dimensional computed tomographic angiography (3D-CTA), have detected unruptured cerebral aneurysms with high sensitivity (26). Although some previous studies focus on aneurysm diameter and location to predict aneurysm rupture, these simple parameters have limitations, including its poor interaction with hemodynamic variables (24, 27). Indeed, recent studies using computational fluid dynamic (CFD) techniques have demonstrated that hemodynamic features are possible key parameters for aneurysm growth and rupture (1-4, 8, 11, 12, 17, 18, 21-23, 28). If hemodynamic factors contribute to aneurysm rupture as reported previously, it is hypothesized that there would be unique hemodynamic features around the rupture point. To our knowledge, however, local hemodynamic features of rupture sites have not been previously or fully examined with CFD analysis. Thus, the goal of the present study was to use CFD analysis based on patient-specific models obtained from preoperative 3D-CTA to characterize the relationship between hemodynamic features and the aneurysmal rupture point observed during microsurgical clipping.

METHODS

Patient Population

From April 2007 to March 2010, 60 ruptured middle cerebral artery (MCA) aneurysms were diagnosed by 3D-CTA, and clipping surgeries were performed in 58 cases. Among them, 12 aneurysms ranging in size from 3.3 to 13.6 mm (mean size, 7.8 mm) were analyzed in this study, because the 12 aneurysms satisfied the following criteria for inclusion: 1) detection of the apparent rupture point during clipping surgery, 2) availability of preoperative 3D-CTA with adequate image quality for generation of a geometry model, and 3) the dome volume that could be distinguished from the middle cerebral parent artery volume through the use of an intersecting plane (Figure 1A) (21). Another 46 aneurysms were excluded due to failed detection of an apparent rupture point during surgery (n = 34) and/or poor imaging quality (n = 12).

Image Acquisition

Preoperative 3D-CTA were performed with a 64-detector multislice computed

REV 5.1.0 DTD ■ WNEU1767_proof ■ 29 April 2013 ■ 7:00 pm ■ ce

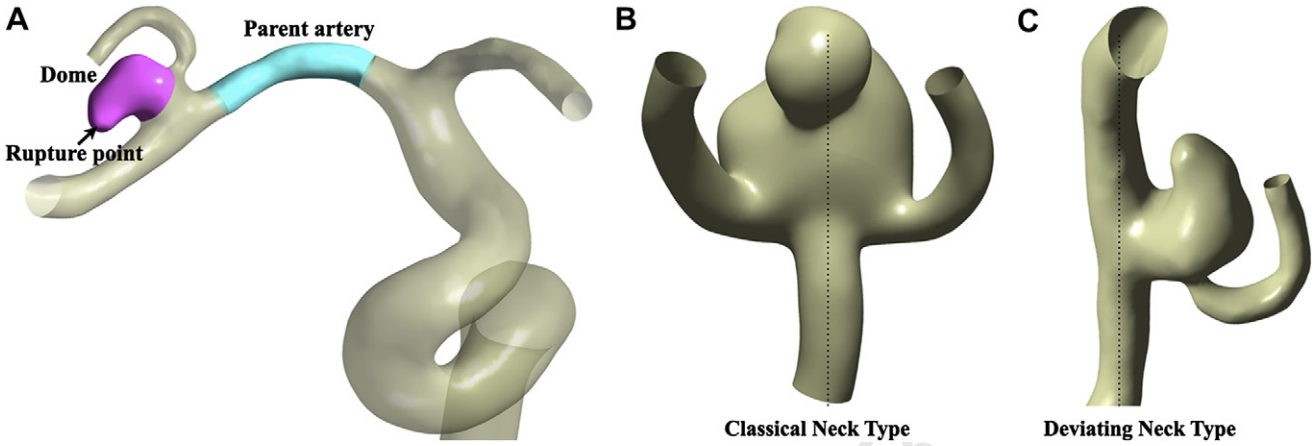

Figure 1. (**A**) Definition of neck geometry; (**B**) classic neck type, showing that the central axis of the parent artery crosses the line of the neck; (**C**) deviating neck type, showing that the central axis of the parent artery does not cross the line of the neck.

tomography (CT) scanner (Aquillion 64; Toshiba, Inc., Tokyo, Japan). Study parameters included radiation parameters 300 mA and 120 kV, matrix size 512 × 512, field of view 32 cm, slice thickness 0.5 mm, helical pitch 1.0, and isotropic voxel size 0.5 mm. A 100-mL dose of nonionic contrast medium (Omnipaque 370; Daiichi-Sankyo Pharmaceutical Co., Tokyo, Japan) was delivered into the right antecubital vein by means of a power injector at the rate of 5 mL/s. The initiation of scanning was set with a real-time bolus-tracking system (Sure Start; Toshiba, Inc., Tokyo, Japan). For each aneurysm, the neck width and the maximum height of the dome were measured from the 3D-CTA, and the aspect ratio (25) was determined.

Model Construction

The surface of the arterial lumen was constructed first by using commercially available software packages (Magics 13.0 and Mimics 14.0; Materialise Japan, Yokohama, Japan). Arterial lumen was segmented based on intra-arterial CT values to convert the Digital Imaging and Communication in Medicine dataset into stereolithography. In addition, smoothing of Laplace transform was performed. The surface geometry was divided into dome and parent artery with an intersecting plane (Figure 1A). The computational meshes were generated for these models using commercial software (ANSYS ICEM CFD12.1; ANSYS Inc., Canonsburg, PA, USA). Element sizes ranged between 0.1 and 0.7 mm, with smaller elements in high curvature regions. Three prismatic boundary layers with a total thickness of 0.15 mm covered the vessel wall to locally ensure an accurate definition of the velocity gradient. A straight inlet extension was added to the C_5 segment of the internal carotid artery to obtain fully developed laminar flow. On average, meshes consisted of 230,000 nodes and 580,000 tetrahedral and prismatic elements.

Numerical Modeling

For the fluid domain, 3D incompressible laminar flow fields were obtained by solving the continuity and Navier-Stokes equations. Numerical modeling was performed using a commercially available CFD package (ANSYS CFX12.1; ANSYS Inc., Canonsburg, PA, USA). Vessel walls were assumed to be rigid, and no slip boundary conditions were applied at the walls. Blood was assumed to be an incompressible Newtonian fluid with a blood density of 1056 kg/m^3 and a blood dynamics viscosity of 0.0035 N/m^2/s. Because patient-specific flow information was not available, pulsatile boundary conditions were based on the superposition blood-flow waveforms of the common carotid artery as characterized by Doppler ultrasound in normal human subjects for transient analysis (9). Traction-free boundary conditions were applied at outlets of the MCA and the anterior cerebral artery (20). The time steps were 0.005 seconds. To reduce initial transients, we computed 3 cardiac cycles, and data of the third cardiac cycle were analyzed. Hemodynamic results of the flow field were examined at end-diastole.

Definition of Geometry

Three independent neurosurgeons evaluated the operation videos blindly to the CFD findings. The rupture point was detected as tight adhesion to hematoma or white thrombus, thin wall, and disruption of the aneurysmal wall (10). After the detection of a rupture point on the operation video, each neurosurgeon determined each location of the rupture point on the patient-specific geometry model. Apparent differences in assessment were resolved by consensus, and if differences were not resolved by consensus, the cases were excluded from the study. The dome was cut around the neck with the intersecting plane, and the M1 segment was defined as the parent artery (Figure 1A). In addition, neck types were classified into 2 types based on neck location. Thus, when the aneurysmal neck was located on the extension of the midline axis of the parent artery, it was defined as a classic neck type (Figure 1B), and when it was not, it was defined as a deviating neck type (Figure 1C). In deviating neck types, relationships among a rupture point, the side of a deviating neck, and the flow dynamics were investigated.

Flow Structure Analysis

Flow structures were investigated with a cross-sectional vector velocity plane including the rupture point and with 3D streamlines of intra-aneurysmal flow.

The number of vortices was counted based on the cross-sectional vector velocity. The area of the proximal M1 segment was calculated for each model, and 80 sampling points/mm² were set at the proximal M1 segment as equally spaced starting points of 3D streamlines. The flow structure was classified into a complex and a simple flow structure. Complex indicates flow structures showing flow separation within the dome and/or containing multiple vortices (3). Simple indicates flow structures without flow separation that contain 1 vortex. Two independent radiologists evaluated these data by means of consensus.

Statistical Analysis

Wall shear stress (WSS) values were recorded at the rupture point, the dome, and the parent artery. WSS at the rupture point was the mean value at the rupture points as defined by 3 neurosurgeons. In addition, minimum WSS at the dome was calculated. Low WSS area was defined as the areas of the aneurysmal wall exposed to a WSS < 10% of the WSS at the parent artery. Because the inlet condition was not patient-specific information, normalized WSS (NWSS), which was the WSS ratio to the WSS magnitude of the parent artery, was used to allow comparisons among different patients. Statistical analysis of the average NWSS at each region was performed using a paired Student t test. Pearson correlation coefficients were calculated between the morphologic parameters and the hemodynamic variables at both the rupture point and the aneurysm dome. Statistical significance was considered present if $P < .05$.

RESULTS

WSS at Rupture Points

The average WSS was significantly lower at the dome (2.27 Pa) than at the parent artery (8.19 Pa, $P < .01$; Table 1). However, WSS was even lower at the rupture point (0.29 Pa) than at the dome ($P < .01$). NWSS was also significantly lower at the rupture point (0.04) than at the dome (0.32, $P < .01$). Rupture points were located within the area of low WSS (<10% of WSS at the parent artery) in 10 of 12 aneurysms, and WSS of rupture points in the remaining 2 aneurysms was 10.8% and 11.2% of WSS at the parent artery. Distribution of WSS in 4 representative cases is shown in Figure 2.

Morphological versus Hemodynamic Variables

The maximum dome height was 7.8 ± 3.8 mm, and the aspect ratio was 1.93 ± 1.07 (Table 1). NWSS at the rupture point significantly correlated with the relative area of low WSS to dome ($r = 0.65$, $P < .05$) and the minimum WSS at the dome ($r = 0.64$, $P < .05$). However, NWSS at the rupture point did not correlate with any morphological variables, including dome height ($r = 0.26$) or the aspect ratio ($r = 0.16$; Figure 3). By contrast, NWSS at the dome correlated with morphological variables (dome height, $r = 0.63$, $P < .05$; aspect ratio, $r = 0.61$, $P < .05$), as well as the relative area of low WSS to dome ($r = 0.76$, $P < .01$), but did not correlate with the minimum WSS at the dome ($r = 0.54$) or the NWSS at the rupture point ($r = 0.57$; Figure 4).

Flow Characteristics of Rupture Points and Neck Types

Flow pattern analysis based on 3D streamlines of intra-aneurysmal flow and cross-sectional flow vector velocity planes showed that 11 aneurysms (91.7%) had a complex flow structure. Among 11 aneurysms with complex flow pattern, 6 aneurysms had flow separation near the rupture points. In 10 aneurysms with multiple vortices, the recirculation flow was observed near the rupture points, and its vector velocity was lower than the velocity of other vortices.

Table 1. Summary of Morphological Parameters, Hemodynamic Values, and Flow Pattern.

Case Number	DH (mm)	AR	DA (mm²)	LWSSA (mm²)	Neck Type	WSSr (Pa)	WSSd (Pa)	WSSp (Pa)	minWSSd (Pa)	NV	FS	Flow Type
1	3.3	1.43	14.8	4.0	CN	0.12	4.43	9.63	0.02	1	1	Complex
2	10.5	2.33	93.5	47.9	CN	0.21	1.28	9.69	0.01	2	1	Complex
3	8.1	1.09	181.2	29.2	CN	0.10	2.13	5.14	0.03	2	1	Complex
4	13.6	1.63	231.7	79.2	CN	0.05	0.75	3.57	0.02	2	1	Complex
5	3.4	1.17	27.9	0.3	DN	0.98	4.45	9.10	0.27	1	0	Simple
6	5.4	1.06	82.7	12.8	DN	0.32	1.51	4.00	0.03	2	0	Complex
7	7.8	2.23	109.2	53.0	DN	0.04	1.27	6.66	0.01	2	0	Complex
8	11.8	3.34	155.8	12.2	DN	0.88	2.66	7.87	0.03	2	0	Complex
9	7.1	1.75	79.0	21.2	DN	0.22	1.84	10.67	0.03	2	1	Complex
10	13.9	4.58	290.2	281.2	CN	0.00	0.18	14.32	0.00	3	0	Complex
11	4.1	1.32	37.3	2.9	DN	0.28	4.05	14.17	0.03	2	1	Complex
12	5.2	1.25	35.1	1.3	CN	0.26	2.69	3.44	0.11	2	1	Complex
Average	7.8	1.93	111.5	45.4		0.29	2.27	8.19	0.05	1.9	0.6	
SD	3.8	1.07	86.9	78.2		0.32	1.43	3.79	0.08	0.5	0.5	

DH, dome height; AR, aspect ratio; DA, dome area; LWSSA, low wall shear stress area; WSSr, WSS at rupture point; WSSd, WSS at dome; WSSp, WSS at parent artery; minWSSd, minimum WSS at dome; NV, number of vortices; FS, flow separation; CN, classic neck; DN, deviating neck; SD, standard deviation.

REV 5.1.0 DTD ■ WNEU1767_proof ■ 29 April 2013 ■ 7:00 pm ■ ce

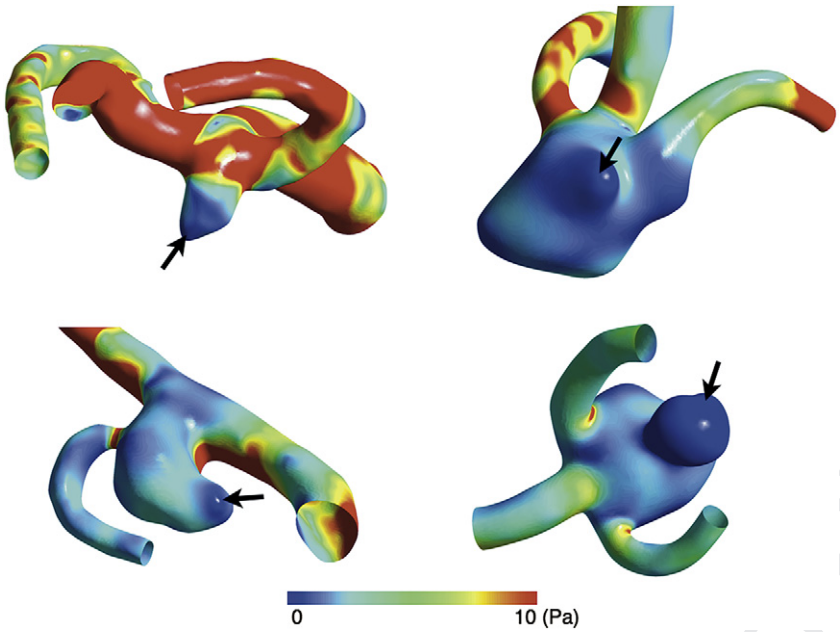

Figure 2. Wall shear stress distribution for 4 representative ruptured middle cerebral artery aneurysms. *Arrows* show the rupture points.

Deviating neck types were observed in 6 aneurysms (Table 1). One aneurysm with a simple flow structure had a deviating neck. Rupture points of all 6 aneurysms with deviating necks were observed on the opposite side of the neck deviation. Irrespective of flow structure and aneurysm neck types, blood flow velocity around the rupture point was low, accounting for low WSS.

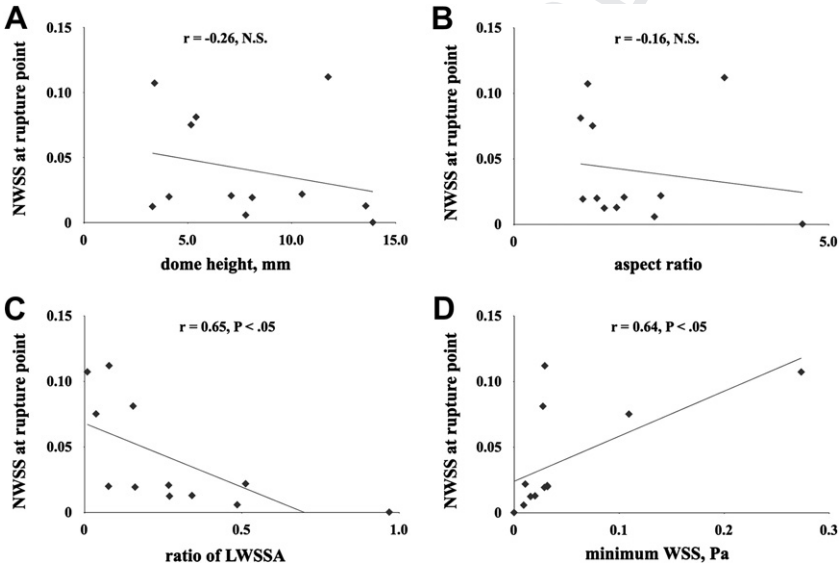

Figure 3. Scattergram with regression analysis of normalized wall shear stress (NWSS) at rupture points. NWSS at the rupture point does not correlate with the dome height (**A**) or the aspect ratio (**B**). By contrast, NWSS at the rupture point correlates with the ratio of the low WSS area (LWSSA) to the dome (**C**) and with the minimum WSS at the dome (**D**). NS, not significant.

Representative Cases

Case 1. The rupture point in this case occurred at the tip of the aneurysm dome within the low WSS area (Figure 5A, 5B). The dome had flow separation, although only 1 flow vortex was observed within the dome. Both 3D streamlines (Figure 5C) and cross-sectional vectors (Figure 5D) of blood flow velocity showed that the rupture point was located at the area of low flow velocity, apart from the impact zone of blood flow.

Case 3. This case (Figure 6), with a rupture point that was around the neck of the aneurysm and within the low WSS area, had a flow separation and 2 flow vortices within the dome. The flow vortex around the rupture point had an obviously lower flow velocity than the other vortex, accounting for low WSS.

Case 9. This case (Figure 7) had a deviating neck. The cross-sectional flow vector velocity plane including the rupture point showed that flow velocity around the rupture point was lower than that of other areas.

DISCUSSION

Local Hemodynamic Features Around the Rupture Point

Based on the microsurgical characterization of 12 ruptured MCA aneurysms, the present study first demonstrated unique local hemodynamic features around the rupture point that were not related to the aneurysm morphology. The magnitude of the WSS was markedly lower at the rupture point than at the dome, and the blood flow velocity was low, associated with complex flow structures and/or deviating necks.

Role of WSS

Experimental studies suggest that aneurysmal behavior is modulated by WSS, which is transduced via mechanoreceptors on endothelial cells to modulate intracellular signaling cascades and gene expression (8, 11, 14, 15, 21). A number of CFD studies have demonstrated that low WSS at the entire dome and/or larger area of low WSS at the dome are associated with aneurysm rupture (12, 21). A recent study also suggested that hemodynamics were as important as morphology in assessing the risk of aneurysm rupture, and that

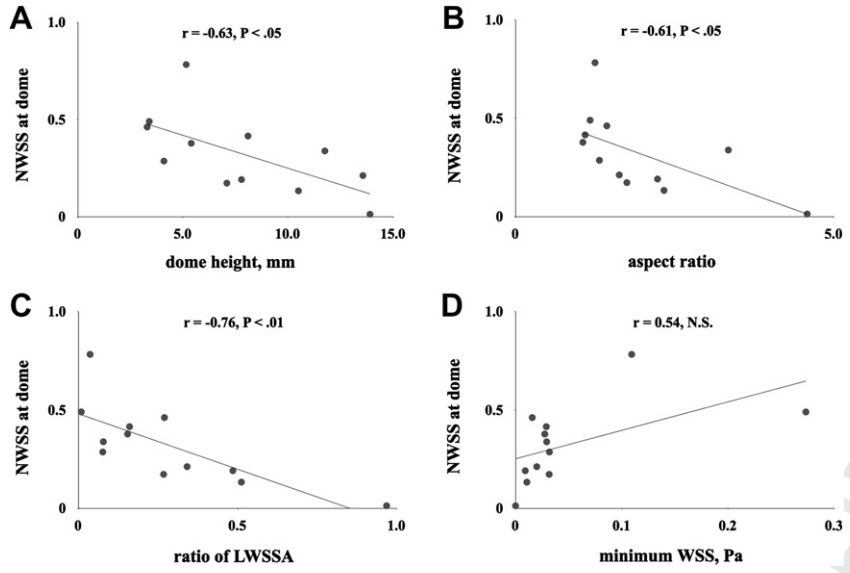

Figure 4. Scattergram with regression analysis of normalized wall shear stress (NWSS) at the dome. NWSS at the dome correlates with the dome height (**A**), the aspect ratio (**B**) and the ratio of the low WSS area (LWSSA) to the dome (**C**). However, NWSS at the dome does not correlate with the minimum WSS at the dome (**D**). NS, not significant.

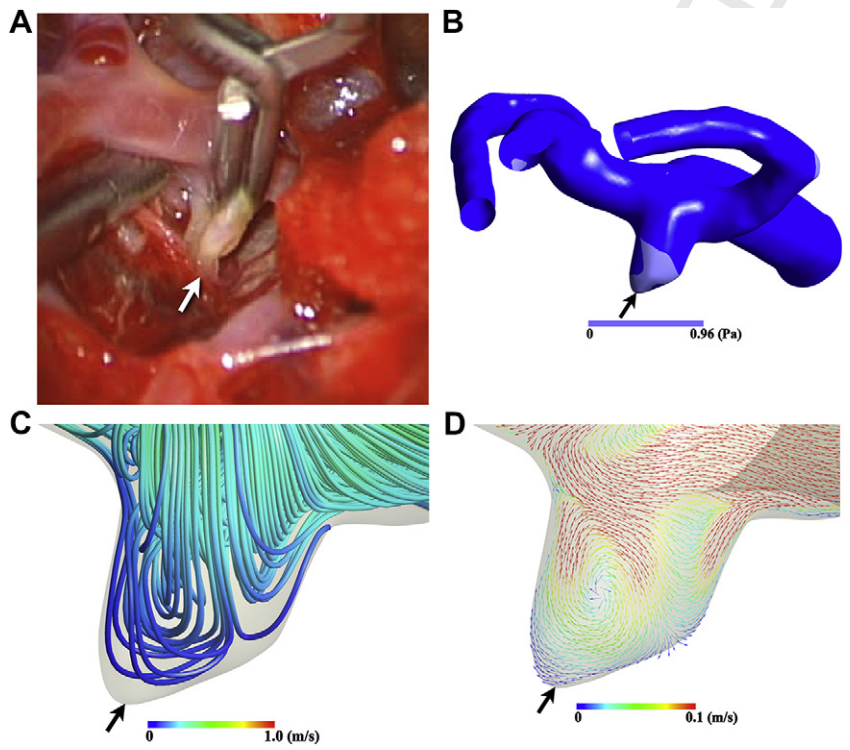

Figure 5. Representative case of a rupture point detected at the aneurysm tip (Case 1). (**A**) Intraoperative photography after the tentative clipping shows the tight adhesion (*white arrow*) between the aneurysm tip (rupture point) and the hematoma; (**B**) the rupture point is observed within the low wall shear stress area; (**C**) flow separation is detected on 3-dimension streamlines of intra-aneurysmal flow; (**D**) the cross-sectional flow vector velocity plane shows the lower velocity around the rupture point. *Black arrow*, rupture point.

WSS was one of the most significant hemodynamic factors (16, 28). The present study first demonstrated that the magnitude of NWSS at rupture points was much lower than that of the NWSS at the dome, and that the WSS at the rupture point was correlated with the minimum WSS at the dome. Moreover, WSS at the rupture point was not correlated with aneurysm size and the aspect ratio. These results suggest that lower WSS would be a significant component contributing to the degenerative process ongoing in the aneurysm wall and aneurysm rupture, independent of aneurysm morphology, although further studies are needed to confirm this hypothesis and to examine the possible contribution of other factors.

Flow Pattern at Rupture Points

A rupture point exists typically at the aneurysm tip (Figure 5), but sometimes at the lateral wall of the dome (Figure 6) (5, 6). Although the location of rupture points is different, our results first revealed that all rupture points are characterized by low WSS magnitude and lower flow velocity. Local lower blood flow velocity may cause low WSS at the rupture point.

The flow pattern has been reported to be a possible key factor related to the pathological mechanism of aneurysm rupture (3). Complex flow patterns can be interpreted as an intermittent localized flow stagnation, possibly leading to the apoptosis of endothelial cells, the release of several chemical mediators, and inflammatory reactions (7, 13). In this study, 11 of 12 aneurysms had complex flow patterns and 10 aneurysms had multiple vortices in which the recirculation flow was observed near the rupture points and the flow velocity was lower than the velocity of other vortices. Therefore, complex flow patterns also can characterize ruptured aneurysms or rupture points, but further studies are needed to confirm whether the flow pattern is the cause, result, or epiphenomenon of aneurysm rupture.

Aneurysm Neck Position

Previous CFD studies suggest that aneurysms with a deviating neck are associated with aneurysm rupture (19). In this study, deviating necks were observed only in 6 of 12 ruptured aneurysms. In all aneurysms with deviating necks, however, rupture

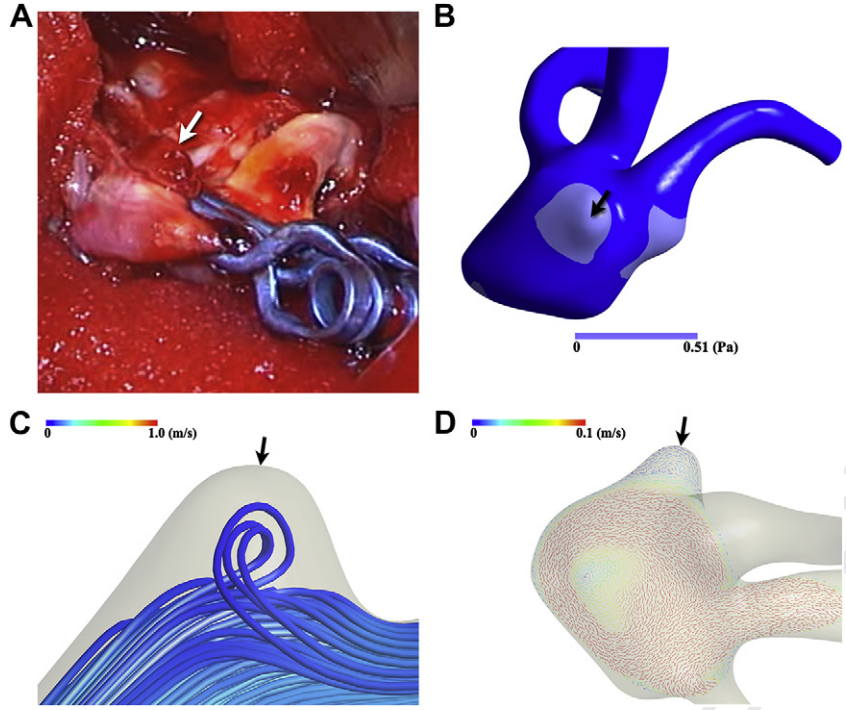

Figure 6. Representative case of a rupture point detected at the aneurysm body (Case 3). (**A**) Intraoperative photography after the neck clipping shows the residual hematoma (*white arrow*) at the aneurysm body (rupture point); (**B**) the rupture point is observed within the low wall shear stress area; (**C**) 3-dimensional streamlines of intra-aneurysmal flow show the flow separation; (**D**) there are 2 vortices in the cross-sectional flow vector velocity plane, and the flow velocity of the vortex near the rupture point is markedly lower than that of the other vortex. *Black arrow*, rupture point.

points were located at the opposite side of the deviating neck. The flow velocity and WSS were also low near the rupture point. Therefore, we can speculate that a deviating neck may contribute to flow stagnation or complex flow, leading to lower flow velocity and WSS, which may characterize a rupture point.

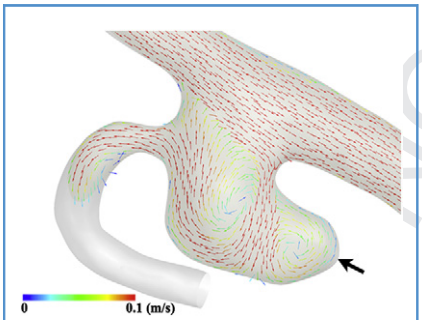

Figure 7. Cross-sectional flow vector velocity plane including a rupture point for a representative case with a deviating neck (Case 9). Flow velocity around the rupture point (*black arrow*) is lower than that of other areas.

Determination of Rupture Point by CFD

Past pathological studies demonstrated that although most aneurysms rupture at the tip, some rupture at the lateral wall of the dome or around the neck (5, 6). Thus, determination of rupture points is often difficult preoperatively. However, this study showed that CFD can detect a rupture point by features such as markedly low WSS and near the complex flow. In contrast, in a clinical setting, the structure of ruptured aneurysms is often multilobular or irregular in shape, and the aneurysm tip may not always be localized. In such a case, an aneurysm may have multiple blebs with similar flow dynamic features. We speculate that a bleb with the lowest WSS may be a rupture point in the case. We should study the issue in the next project.

Limitations of the Study

First, this study required the overlay of the rupture point identified during microsurgery on the patient-specific geometry model. The procedure can cause a certain bias because of converting the abstract information of the rupture point into the digital data of 3D images, although 3 experienced neurosurgeons determined the rupture point independently and blindly. Secondly, histopathological examination would be advisable for more accurate confirmation of the rupture points on the geometry model and for the determination of the relationships between CFD findings and aneurysm wall fragility. Thirdly, aneurysm rupture itself may affect the configurations of aneurysms. In addition, although 1 study reported that hemostasis of ruptured aneurysms primarily occurs via a platelet plug or fibrin net at the outside surface of the aneurysm rupture point (28), there is a theoretical possibility that this could bias our results. Thus, prospective studies of unruptured aneurysms are needed to determine whether lower WSS can predict the subsequent aneurysm rupture. Lastly, the number of cases included in this study was small, and this study only included bifurcation-type aneurysms. Further studies are necessary to validate the application of CFD to determine the aneurysm rupture point.

CONCLUSIONS

This study suggested that CFD can determine the location of aneurysm rupture points using the characteristic flow dynamic features such as complex flow and markedly low WSS.

REFERENCES

1. Boussel L, Rayz V, McCulloch C, Martin A, Bolton GA, Lawton M, Higashida R, Smith WS, Young WL, Saloner D: Aneurysm growth occurs at region of low wall shear stress: patient-specific correlation of hemodynamics and growth in a longitudinal study. Stroke 39:2997-3002, 2008.

2. Castro MA, Putman CM, Sheridan MJ, Cebral JR: Hemodynamic patterns of anterior communicating artery aneurysms: a possible association with rupture. AJNR Am J Neuroradiol 30:297-302, 2009.

3. Cebral JR, Castro MA, Burgess JE, Pergolizzi RS, Sheridan MJ, Putman CM: Characterization of cerebral aneurysms for assessing risk of rupture by using patient-specific computational hemodynamics models. AJNR Am J Neuroradiol 26: 2550-2559, 2005.

4. Cebral JR, Hendrickson S, Putman CM: Hemodynamics in a lethal basilar artery aneurysm just

before its rupture. AJNR Am J Neuroradiol 30: 95-98, 2009.

5. Crawford T: Some observations on the pathogenesis and natural history of intracranial aneurysms. J Neurol Neurosurg Psychiatr 22:259-266, 1959.

6. Crompton MR, Path MC: Mechanism of growth and rupture in cerebral berry aneurysms. Br Med J 1:1138-1142, 1966.

7. D'Arcangelo D, Ambrosino V, Giannuzzo M, Gaetano C, Capogrossi MC: Axl receptor activation mediates laminar shear stress anti-apoptotic effects in human endothelial cells. Cardiovasc Res 71:754-763, 2006.

8. Hoi Y, Meng H, Woodward SH, Bendok BR, Hanel RA, Guterman LR, Hopkins LN: Effect of arterial geometry on aneurysm growth: three-dimensional computational fluid dynamics study. J Neurosurg 101:676-681, 2004.

9. Holdsworth DW, Norley CJD, Frayne R, Steinman DA, Rutt BK: Characterization of common carotid artery blood-flow waveforms in normal human subjects. Physiol Meas 20:219-240, 1999.

10. Ishikawa T, Nakayama N, Yoshimoto T, Yoshimoto T, Aoki T, Terasaka S, Nomura M, Takahashi A, Kuroda S, Iwasaki Y: How does spontaneous hemostasis occur in ruptured cerebral aneurysms? Preliminary investigation on 247 clipping surgeries. Surg Neurol 66:269-276, 2006.

11. Isoda H, Takeda H, Yamashita S, Takehara Y, Sakahara H, Hiramatsu H, Nanba H, Hirano M, Okuhara Y, Kosugi T, Alley MT: Hemodynamic analysis of intracranial aneurysms. No Shinkei Geka 37:836-845, 2009.

12. Jou L-D, Lee DH, Morsi H, Mawad ME: Wall shear stress on ruptured and unruptured intracranial aneurysms at the internal carotid artery. AJNR Am J Neuroradiol 29:1761-1767, 2008.

13. Keulenaer GWD, Chappell DC, Ishizaka N, Nerem RM, Alexander RW, Griendling KK: Oscillatory and steady laminar shear stress differentially affect human endothelial redox state: role of a superoxide-producing NADH oxidase. Circ Res 82:1094-1101, 1998.

14. Li YJ, Haga JH, Chien S: Molecular basis of the effect of shear stress on vascular endothelial cells. J Biomech 38:1949-1971, 2005.

15. Malek AM, Alper SL, Izumo S: Hemodynamic shear stress and its role in atherosclerosis. JAMA 282:2035-2042, 1999.

16. Meng H, Wang Z, Hoi Y, Gao L, Metaxa E, Swartz DD, Kolega J: Complex hemodynamics at the apex of an arterial bifurcation induces vascular remodeling resembling cerebral aneurysm initiation. Stroke 38:1924-1931, 2007.

17. Montha A, Karmonik C, Benndorf G, Strother C, Metcalfe R: Hemodynamics in a cerebral artery before and after the formation of an aneurysm. AJNR Am J Neuroradiol 27:1113-1118, 2006.

18. Moyle KR, Antiga L, Steinman DA: Inlet conditions for image-based CFD models of the carotid bifurcation: is it reasonable to assume fully developed flow? J Biomech Eng 128:371-379, 2006.

19. Ohshima T, Miyachi S, Hattori K, Takahashi I, Ishii K, Izumi T, Yoshida J: Risk of aneurismal rupture: the importance of neck orifice positioning-assessment using computational flow simulation. Neurosurgery 62:767-775, 2008.

20. Papanastasiou TC, Malamataris N, Ellwood K: A new outflow boundary condition. Int J Numer Meth Fluids 14:587-608, 1992.

21. Shojima M, Ohshima M, Takagi K, Torii R, Hayakawa M, Katada K, Morita A, Kirino T: Magnitude and role of wall shear stress on cerebral aneurysm: computational fluid dynamic study of 20 middle cerebral artery aneurysms. Stroke 35: 2500-2505, 2004.

22. Shojima M, Ohshima M, Takagi K, Torii R, Nagata K, Shirouzu I, Morita A, Kirino T: Role of bloodstream impacting force and the local pressure elevation in the ruptured cerebral aneurysms. Stroke 36:1933-1938, 2005.

23. Steinman DA, Milner JS, Norley CJ, Lownie SP, Holdsworth DW: Image-based computational simulation of flow dynamics in a giant intracranial aneurysm. AJNR Am J Neuroradiol 24:559-566, 2003.

24. The International Study of Intracranial Aneurysms Investigators: Unruptured intracranial aneurysms-risk of rupture and risks of surgical intervention. N Engl J Med 339:1725-1733, 1998.

25. Ujiie H, Tachibana H, Hiramatsu O, Hazel AL, Matsumoto T, Ogasawara Y, Nakajima H, Hori T, Takakura K, Kajiya F: Effects of size and shape (aspect ratio) on the hemodynamics of saccular aneurysms: a possible index for surgical treatment of intracranial aneurysms. Neurosurgery 45: 119-130, 1999.

26. White PM, Teasdale EM, Wardlaw JM, Easton V: Intracranial aneurysms: CT angiography and MR angiography for detection-prospective blinded comparison in a large patient cohort. Radiology 219:739-749, 2001.

27. Wiebers DO: International Study of Unruptured Intracranial Aneurysms Investigators: Unruptured intracranial aneurysms: natural history, clinical outcome, and risk of surgical and endovascular treatment. Lancet 362:103-110, 2003.

28. Xiang J, Natarajan SK, Tremmel M, Ma D, Macco J, Hopkins LN, Siddiqui AH, Levy EI, Meng H: Hemodynamic-morphologic discriminants for intracranial aneurysm rupture. Stroke 42:144-152, 2011.

Conflict of interest statement: The authors declare that the article content was composed in the absence of any commercial or financial relationships that could be construed as a potential conflict of interest.

Citation: World Neurosurg. (2013). http://dx.doi.org/10.1016/j.wneu.2013.02.012

Journal homepage: www.WORLDNEUROSURGERY.org

Available online: www.sciencedirect.com

1878-8750/$ - see front matter